Integral Cross Sections for Electron–Magnesium Scattering Over a Broad Energy Range (0–5000 eV)

Cite as: J. Phys. Chem. Ref. Data **47**, 043104 (2018); https://doi.org/10.1063/1.5081132
Submitted: 15 October 2018 . Accepted: 14 November 2018 . Published Online: 14 December 2018

R. P. McEachran, F. Blanco, G. García, P. W. Stokes, R. D. White, and M. J. Brunger

Integral Cross Sections for Electron–Magnesium Scattering Over a Broad Energy Range (0–5000 eV)

R. P. McEachran
Plasma Research Laboratory, Research School of Physics and Engineering, Australian National University, Canberra, A.C.T. 0200, Australia

F. Blanco
Departamento de Física Atómica, Molecular y Nuclear, Universidad Complutense de Madrid, Avenida Complutense, E-28040 Madrid, Spain

G. García
Instituto de Física Fundamental, CSIC, Serrano 113-bis, E-28006 Madrid, Spain

P. W. Stokes, and R. D. White
College of Science and Engineering, James Cook University, Townsville, Queensland 4810, Australia

M. J. Brunger[a)]
College of Science and Engineering, Flinders University, GPO Box 2100, Adelaide, South Australia 5001, Australia

(Received 15 October 2018; accepted 14 November 2018; published online 14 December 2018)

We report the results from the application of our optical potential and relativistic optical potential (ROP) methods to electron–magnesium scattering. The energy range of this study was 0–5000 eV, with the results for the integral elastic cross sections, summed discrete electronic-state excitation integral cross sections, momentum transfer cross sections, and total ionisation cross sections being reported. Where possible, we compare the present results to the available experimental data and to the earlier results from close coupling and R-matrix type computations. Typically, a quite fair level of accord is found between our ROP calculations and the earlier theoretical and experimental cross sections. Additionally, from the assembled database, we provide for the modeling community some recommended cross section sets for use in their simulations, in which magnesium is a constituent. Electron transport coefficients are subsequently calculated for reduced electric fields ranging from 0.1 to 1000 Td using a multiterm solution of Boltzmann's equation. Substantial differences in the transport coefficients between the ROP calculations and the recommended cross sections are observed over the range of fields considered, clearly illustrating the importance of the veracity of the database in the simulations. *Published by AIP Publishing on behalf of the National Institute of Standards and Technology.* https://doi.org/10.1063/1.5081132

Key words: electron scattering cross sections; electron transport; magnesium; recommended cross sections.

CONTENTS

List of Tables

[a)]Author to whom correspondence should be addressed: michael.brunger@flinders.edu.au
Published by AIP Publishing on behalf of the National Institute of Standards and Technology.

List of Figures

1. Introduction

There has been significant interest in measuring and calculating cross sections for electron–magnesium (Mg) scattering over many years. For elastic and/or discrete excitation processes, we note the experimental studies from The Jet Propulsion Laboratory (JPL),[1] Flinders University,[2–4] and Newcastle University[5,6] and an extensive series of measurements from the Belgrade group.[7–11] For completeness, we also note some electron–photon coincidence studies on the 3^1P state of Mg[5,6,12] and a very recent superelastic experiment on this same electronic state.[13] In terms of the ionisation process, we note total ionisation cross section (TICS) measurement results from Refs. 14–16. From the theoretical perspective, there has been significantly more work, with only the most recent and/or relevant papers now listed. Those studies include B-spline R-matrix (BSR) calculations from the Drake University group,[17–19] convergent close coupling (CCC) calculations from Curtin University,[18–20] and an optical potential (OP) variant[21] on what we report here. Note that there are many more earlier theoretical studies apart from those listed above,[17–21] which the interested reader can find in the reference lists of Refs. 17–21. Of course, at least in part, what made Mg attractive to study is that it can be considered as a quasi-two-electron system, and so, for the theorists, it remained tractable to full quantum mechanical treatments using developed computational methods.

From a more applied perspective, Mg is an element of significant astrophysical importance, being produced by hydrostatic carbon burning in massive stars.[19] Its significant abundance combined with a raft of spectral features across the UV to the IR makes it an important diagnostic in studying stellar and supernova behaviour. This is achieved through non-local thermodynamic equilibrium modeling of the observed spectra, with some examples being the measurement of Mg stellar abundances in cool stars,[22] as a temperature diagnostic of the solar chromosphere,[23] as a probe of velocity fields in giant stars,[24] and in the modeling of supernovae ejecta.[25] In all those modeling applications, accurate and complete[26] electron scattering cross sections form a vital element, as is well documented in the recent paper from Barklem *et al.*[19]

Our own experience of modeling electron transport phenomena,[27–32] including the role of electron-driven processes in planetary atmospheres,[33,34] suggests that quantitative results are only achievable if a complete cross section database over a large incident electron energy range (0–5000 eV) is available. This latter statement provides two of the rationales for the present work. First, along with our present OP and relativistic optical potential (ROP) results, we aim to interrogate the available database in order to provide a set of recommended integral cross sections (ICSs) for elastic scattering, the summed discrete excited electronic states and for the total ionisation process. Second, we seek to provide those data over the energy range 0–5000 eV. In this respect, we note that the electron scattering database employed in Ref. 19 was only over the range 0–100 eV, which is too narrow for most transport or kinetic-radiative application simulations.

The structure for the remainder of this paper is as follows: In Sec. 2, we provide details of our OP and ROP calculations, while in Sec. 3, we present those results and compare them to data from other theories and experiments. In Sec. 4, we detail how we construct our recommended cross section sets for e^-–Mg scattering and list those cross sections in tabular form. Note that a discussion of the uncertainty limits on those recommended data is also provided in this section. We also present calculated transport coefficients over a range of reduced electric fields (E/n_0 where E is the electric field and n_0 is the neutral number density) relevant to the modeling community, highlighting the differences in the macroscopic properties arising from differences in the cross section sets. Finally, in Sec. 5, some conclusions from the present investigation will be given.

2. Theoretical Details

In this section, we provide some brief details in respect to our current OP and ROP theoretical methods and their application to e^-–Mg scattering.

2.1. Optical potential

In order to obtain a complete set of differential and integral elastic as well as integral inelastic cross sections for electron

scattering from Mg atoms in the energy range 0.02–5000 eV, calculations have been performed based on the formulation of suitable OPs, in order to solve the scattering equations for the corresponding complex phase shifts. Details on the application of the corrected quasi-free absorption potential method to electron interactions have been provided in previous studies,[35–37] being most recently applied to Be atoms,[38] so that only a brief description will be given here. The electron–atom scattering process can be represented by the following complex potential:

$$V_{\rm opt}(r) = V_{\rm st}(r) + V_{\rm ex}(r) + V_{\rm pol}(r) + iV_{\rm abs}(r)\,, \qquad (1)$$

where $V_{\rm st}(r)$ is the static potential derived from a standard Hartree–Fock calculation of the atomic charge density, $V_{\rm ex}(r)$ is the exchange potential, $V_{\rm pol}(r)$ is the polarization potential, and $V_{\rm abs}(r)$ is the absorption potential that accounts for the inelastic processes. These potentials are obtained with a similar procedure as that explained in Refs. 35–37. Further to this representation, inelastic processes are due to electron–electron collisions between incident particles and a ''quasi-free'' electron cloud representing the target electrons. Having corrected some deficiencies in the original formulation of Staszewska *et al.*[39] and adding further improvements in the description of the electron's indistinguishability, the inclusion of screening effects, restoring the magnitude of the local velocity vector during the collision process, and including relativistic and many-body corrections (see Ref. 37 for details), we obtained a model which provides a good approximation for electron–atom scattering over a broad energy range.[37] All these improvements are based on first physical principles and no external parameters are used during the calculation procedure. In this sense, it is considered an ''*ab initio*'' calculation procedure. As discussed in Refs. 36 and 37, the energy gap parameter (Δ) is a critical value which represents the threshold energy for considering inelastic processes through the imaginary (absorption) part of the potential. In particular, see Ref. 36, as originally inelastic processes are considered as electron–electron collisions between the incident beam and a free electron cloud representing the target electrons, we could initially consider Δ as the threshold energy to excite continuum states, i.e., the ionisation potential (I). However, we have shown in the aforementioned previous studies[35–37] that defining Δ as the energy of the first optically allowed excited state is an approximate way of accounting for the contribution of the bound state excitation processes. Strictly speaking, this energy gap should correspond to the first excited state, including optically forbidden states which are accessible via electron excitation. However for most atomic targets, the first optically forbidden states have their excitation energy rather close to the ground state and their contribution to the overall excitation processes is quite negligible. Hence considering this energy as the Δ parameter could lead to an overestimation of the total inelastic cross section. Although the criterion of using the first optically allowed excited energy as the threshold energy worked reasonably well in our previous electron–atom calculations,[35–38] the relevance of the first optically forbidden excited states needs to be evaluated for each new target under investigation. Indeed in this case, due to strong configuration mixing in the Mg atom, we did need to use the ^{3}P excitation energy as the threshold energy (2.711 59[19] eV). A strong hint for this being important here is the observation of an intense line at 457.11 nm in the Mg emission spectrum,[40] which can only arise if the ^{3}P state is described by an admixture of triplet and singlet components in the wavefunction.

We used here a standard partial wave expansion procedure. In order to obtain the lth complex partial-wave phase shift η_l, the scattering equation for the radial wavefunctions has been numerically integrated and the details of such a procedure can be obtained from Refs. 35 and 36. Once the corresponding η_l phase shifts are obtained for the above potential [see Eq. (1)], the elastic differential $d\sigma_{\rm elas}/d\Omega$ and integral $\sigma_{\rm elas}$ cross sections result from the expressions

$$\frac{d\sigma_{\rm elas}}{d\Omega} = \frac{1}{4k^2}\left|\Sigma_{l=0}^{l_{\rm max}}(2l+1)\left(e^{2i\eta_l}-1\right)P_l(\cos\theta)\right|^2 \qquad (2)$$

and

$$\sigma_{\rm elas}(E) = \frac{4\pi}{k^2}\Sigma_{l=0}^{l_{\rm max}}(2l+1)\sin^2\eta_l\,, \qquad (3)$$

respectively, and the total scattering cross section ($\sigma_{\rm total}$) results from the optical theorem $\sigma_{\rm total}(E) = \frac{4\pi}{k^2}{\rm Im}(f_{\theta=0})$. The total inelastic cross section, $\sigma_{\rm inelas}(E)$, corresponds to $\sigma_{\rm inelas}(E) = \sigma_{\rm total}(E) - \sigma_{\rm elas}(E)$.

In order to calculate the electron impact ionisation cross section, $\sigma_{\rm ion}(E)$, the above calculation procedure was repeated but using the ionisation energy (IE) as the gap energy parameter (i.e., $\Delta = IE$). In these conditions, only excitation to continuum states above the ionisation threshold is considered. By combining the respective results for both gap energy parameters, summed electronic excitation cross sections ($\sigma_{\rm exci}$) can also be derived from the expression $\sigma_{\rm inelas}(E) = \sigma_{\rm ion}(E) + \sigma_{\rm exci}(E)$.

A summary of the present OP results is given in Table 1, with the plots of its integral elastic cross sections, summed electronic-state cross sections, and the TICS being found in Figs. 1–3, respectively.

2.2. Relativistic optical potential

The other theoretical procedure used here to describe the elastic and inelastic scattering of electrons from magnesium atoms is based upon the ROP method of Chen *et al.*,[41] hereafter referred to as I. This OP is obtained from an approximate solution of the relativistic close coupling equations. Only a brief discussion of the overall method needs to be given here and the reader is referred to I for the details.

The scattering of the incident electrons, with wavenumber k, by magnesium atoms can be described by the integral equation formulation of the partial wave Dirac-Fock scattering equations. In the ROP method, these equations can be expressed in matrix form as

TABLE 1. A selection of the present theoretical OP results ($\times 10^{-16}$ cm^2) for electron scattering from Mg

Energy (eV)	Elastic ($\times 10^{-16}$ cm^2)	Inelastic ($\times 10^{-16}$ cm^2)	TICS ($\times 10^{-16}$ cm^2)	Total ($\times 10^{-16}$ cm^2)
0.02	59.563 308	0	0	59.563 308
0.03	75.459 16	0	0	75.459 16
0.04	102.232 228	0	0	102.232 228
0.05	146.381 172	0	0	146.381 172
0.07	305.877 404	0	0	305.877 404
0.1	774.475 632	0	0	774.475 632
0.15	1003.468 536	0	0	1003.468 536
0.2	683.924 332	0	0	683.924 332
0.3	406.714 056	0	0	406.714 056
0.4	306.710 404	0	0	306.710 404
0.5	256.011 084	0	0	256.011 084
0.7	202.348 02	0	0	202.348 02
1	161.490 84	0	0	161.490 84
1.5	126.120 316	0	0	126.120 316
2	105.611 968	0	0	105.611 968
3	81.323 508	0	0	81.323 508
4	66.851 484	0.043 4	0	66.894 884
5	56.788 536	1.213 128	0	58.001 664
7	43.045 184	5.136 404	0	48.181 588
10	30.187 22	10.413 48	0.399 028	40.999 728
15	19.946 724	10.070 34	3.610 124	33.627 188
20	15.181 516	8.297 968	5.312 384	28.791 868
30	10.971 884	6.373 976	5.995 5	23.341 36
40	9.019 696	5.411 672	5.767 972	20.199 34
50	7.816 928	4.791 164	5.417 58	18.025 672
70	6.360 424	3.981 516	4.751 292	15.093 232
100	5.141 192	3.281 88	3.956 736	12.379 808
150	4.017 58	2.619 344	3.117 268	9.754 192
200	3.348 464	2.212 728	2.610 132	8.171 324
300	2.558 752	1.726 732	2.013 732	6.299 216
400	2.101 764	1.437 996	1.674 176	5.213 936
500	1.799 98	1.246 224	1.447 488	4.493 692
700	1.419 376	1.004 248	1.160 068	3.583 692
1000	1.097 124	0.801 304	0.916 048	2.814 476
2000	0.651 924	0.526 148	0.571 172	1.749 244
3000	0.474 46	0.415 324	0.424 788	1.314 572
5000	0.313 068	0.304 696	0.284 368	0.902 132

$$\begin{pmatrix} F_\kappa(r) \\ G_\kappa(r) \end{pmatrix} = \begin{pmatrix} v_1(kr) \\ v_2(kr) \end{pmatrix} + \frac{1}{k}\int_0^r dx\, G(x,r) \left[U(x) \begin{pmatrix} F_\kappa(x) \\ G_\kappa(x) \end{pmatrix} - \begin{pmatrix} \overline{W}_P(\kappa;x) \\ \overline{W}_Q(\kappa;x) \end{pmatrix} - i\, U_{\rm opt}(r) \begin{pmatrix} F_\kappa(x) \\ G_\kappa(x) \end{pmatrix} \right], \tag{4}$$

where the local potential $U(r)$ is given by the sum of the static and a local polarization potential, i.e.,

$$U(r) = U_{\rm st}(r) + U_{\rm pol}(r)\,. \tag{5}$$

Here we have followed the procedure given in Refs. 42 and 43 and have replaced the real part of the OP by a local polarization potential based upon the polarized-orbital method of McEachran *et al.*[44,45] The static potential was determined in the usual manner from the Dirac-Fock orbitals of magnesium while the polarization potential $U_{\rm pol}(r)$ in Eq. (5) comprised the sum of the first 7 static polarization potentials plus the corresponding dynamic polarization potential. In particular, the static polarization potentials were determined using the polarized-orbital method,[44,45] while the dynamic polarization potential was determined by the method described in Refs. 46 and 47. Furthermore, the polarized-orbital method yielded a large dipole polarizability of 81.15 a_0^3, and hence, our static dipole polarization potential was scaled to give a dipole polarizability of 70.76 a_0^3.[48] In Eq. (4), $\overline{W}_{P\,{\rm or}\,Q}$ are the large and small components of the non-local exchange terms obtained by antisymmetrisation of the total scattering wavefunction [see Eqs. (22a) and (22b) of I], while the non-local potential $U_{\rm opt}(r)$ denotes the imaginary part of the OP and describes the absorption of the incident flux into the inelastic channels and thereby describes excitation and ionisation processes. This potential is given by a sum and integration over the bound and continuum states of the atom [see Sec. 2.2.1 as well as Eq. (21b) of I for details].

Finally, in Eq. (4), $F_\kappa(r)$ and $G_\kappa(r)$ are the large and small components of the complex scattering wavefunction, while the functions $v_1(kr)$ and $v_2(kr)$ are the corresponding free particle wavefunctions and are given in terms of Riccati-Bessel functions. $G(r, x)$ is the free particle Green's function which can be expressed in matrix form in terms of the Riccati-Bessel and Riccati-Neumann functions [see Eqs. (23), (24a), and (24b) of I for details]. The subscript κ on the scattering wavefunctions is the relativistic angular momentum quantum number of the incident electron. It is related to the

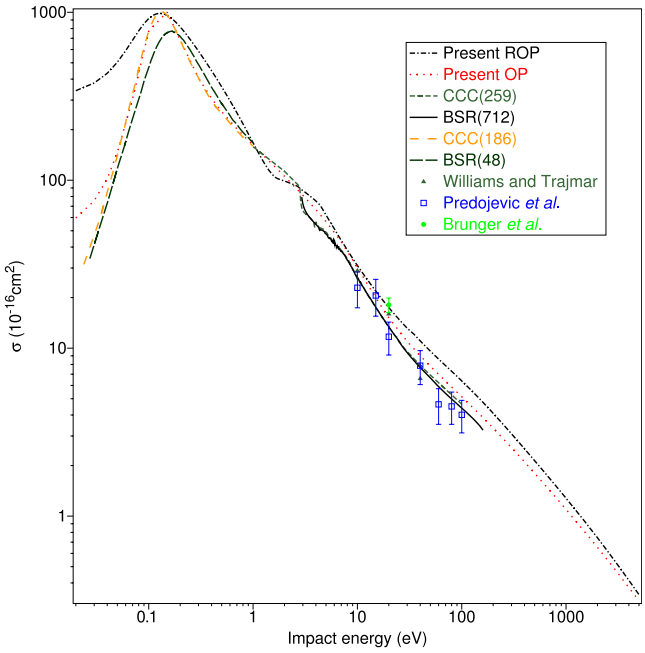

FIG. 1. A selection of the available experimental and theoretical elastic ICS results, including our new OP and ROP results. See the legend for further details.

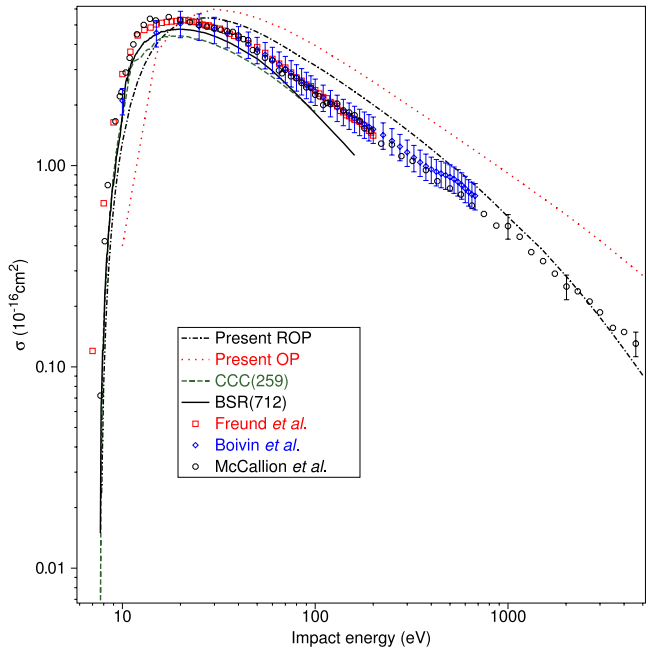

FIG. 3. A selection of the available experimental and theoretical total ionisation cross section results, including our new OP and ROP results. See the legend for further details.

corresponding orbital angular momentum quantum number l according to $\kappa = -l - 1$ when $j = l + \frac{1}{2}$ (spin-up) and $\kappa = l$ when $j = l - \frac{1}{2}$ (spin-down) where j is the total angular momentum quantum number of the incident electron.

Asymptotically, $F_\kappa(r)$ is given by

$$F_\kappa(r)_{r\to\infty} \to \sin\left(kr - \frac{l\pi}{2}\right) + T_l^{\pm}(k)\exp\left(kr - \frac{l\pi}{2}\right), \quad (6)$$

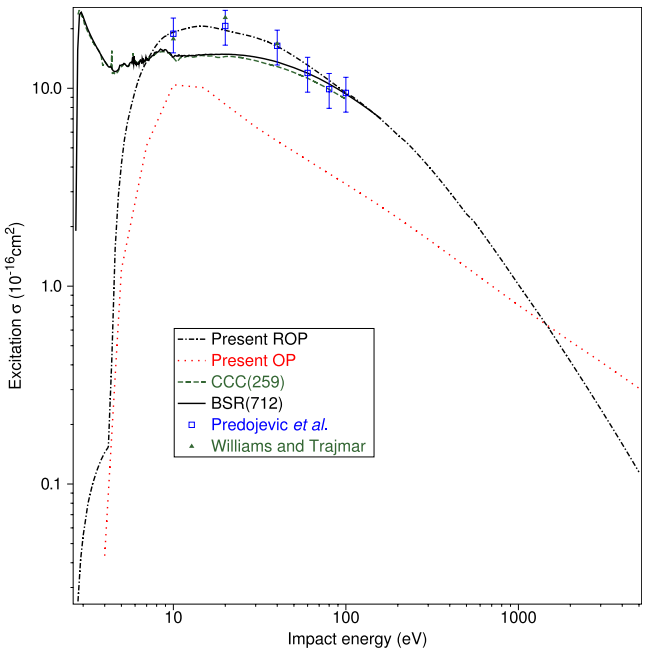

FIG. 2. A selection of the available experimental and theoretical summed electronic-state excitation ICS results, including our new OP and ROP results. See the legend for further details.

where $T_l^{\pm}(k)$ are the complex T-matrix elements. These T-matrix elements can, in turn, be expressed in terms of the complex phase shifts $\eta_l^{\pm}(k)$ according to

$$T_l^{\pm}(k) = \frac{1}{2i}\left[\exp\left(2i\eta_l^{\pm}(k)\right) - 1\right], \quad (7)$$

where the real and imaginary parts of the phase shifts are given by

$$\eta_l^{\pm}(k) = \delta_l^{\pm}(k) + i\,\gamma_l^{\pm}(k). \quad (8)$$

Here the superscript + refers to "spin up" while the superscript − refers to "spin down." In terms of these real and imaginary parts of the phase shifts, the integrated elastic cross section is given by

$$\sigma_{\rm el}(k^2) = \frac{2\pi}{k^2}\sum_{l=0}^{\infty}\left\{(l+1)\exp\left(-2\gamma_l^+\right)\left[\cosh 2\gamma_l^+ - \cos 2\delta_l^+\right] + l\exp\left(-2\gamma_l^-\right)\left[\cosh 2\gamma_l^- - \cos 2\delta_l^-\right]\right\} \quad (9)$$

while the total inelastic or absorption cross section is given by

$$\sigma_{\rm inel}(k^2) = \frac{\pi}{k^2}\sum_{l=0}^{\infty}\left\{(l+1)\left[1 - \exp\left(-4\gamma_l^+\right)\right] + l\left[1 - \exp\left(-4\gamma_l^-\right)\right]\right\}. \quad (10)$$

2.2.1. The optical potential

For magnesium, the following 10 bound excited states, in intermediate coupling notation, were included in $U_{\rm opt}(r)$,

namely, $3p[3/2]^o_1$, $3\overline{p}[1/2]^o_1$, $4p[3/2]^o_1$, $4\overline{p}[1/2]^o_1$, $5p[3/2]^o_1$, $5\overline{p}[1/2]^o_1$, $6p[3/2]^o_1$, $6\overline{p}[1/2]^o_1$, $7p[3/2]^o_1$, and $7\overline{p}[1/2]^o_1$ in order to simulate excitation processes. Also included in $U_{opt}(r)$ were all continuum states with orbital angular momentum given by $l_c = 0, 1, 2, 3$, and 4, in order to simulate ionisation processes. The integration over the continuum states in the absorption potential was approximated by using Gauss-Legrendre integration usually with 16–24 points. The continuum channels also included the ionisation of 2p and $2\overline{p}$ electrons at 54 eV and a 2s electron at 92 eV. In a relativistic close coupling expansion, it is necessary to couple the total angular momentum of the electron in the excited state (bound or continuum) to the total angular momentum of the incident electron to obtain the total angular momentum J of the electron–atom system. This total angular momentum J is then conserved during the collision process. Under the above circumstances, this gave rise to a maximum of 30 excitation channels and 247 ionisation channels in $U_{opt}(r)$.

A summary of the ROP results, including the momentum transfer cross sections (MTCSs), is given in Table 2, with the plots of its integral elastic cross sections, summed electronic-state cross sections, and the TICS being found in Figs. 1–3 respectively.

3. Results and Discussion

In Fig. 1, we plot the present OP and ROP integral elastic cross sections and where possible compare them to the results from the available experimental data[1,2,7] and earlier theoretical close coupling (CCC) and R-matrix (BSR) computations.[18,19] All six theoretical ICS results show the same main semi-quantitative features. Namely, the cross section rises significantly in magnitude from 0 eV to ~0.15 eV where the peak of a p-wave resonance feature[18,49] has a very large cross section magnitude of $\sim 1000 \times 10^{-16}$ cm^2. This resonance feature was first observed in the electron transmission spectrum (ETS) of Burrow *et al.*,[50] who found it to occur at an energy of 0.15 eV. This value is in excellent agreement with what we found from our OP and ROP results and from the CCC 186-state [CCC(186)] calculation. The BSR(48) computation found the resonance peak at a slightly higher energy, but this probably simply reflects the smaller number of states in their basis compared to that employed in the CCC. Above 0.15 eV, all the available calculations [OP, ROP, CCC(186), CCC(259), BSR(48), and BSR(712)] show that the magnitude of the elastic ICS decreases significantly with the increasing energy of the incident electron (note the log axis scale). Interestingly, our ROP result indicates a plateau structure in the elastic ICS at around 3 eV. This corresponds well to a resonance feature in the ETS[50] between 2.5 and 3 eV, which they associate with the opening of the 3^3P electronic-state of Mg. While we cannot definitively assert that the plateau in our ROP calculation is the result of this same resonance, it is plausible that it will be. Between 10 and 100 eV, we can now compare all the theoretical results to the experimental data. We note that the available data[1,2,7] do exhibit some scatter, agreeing with the OP and ROP results better at some energies and with the CCC and BSR results at others. Further complicating this comparison is that all the experimental ICSs were derived from DCS measured over a finite angular range. This means that those DCS need to be extrapolated to 0° and 180° before integration to derive the ICS. As the elastic DCS are all strongly peaked at the more forward scattered electron angles, such an extrapolation is difficult, possibly subjective, and may introduce important uncertainties into the derived experimental ICS. We note that Brunger *et al.*[2] tried to avoid this problem by applying the modified complex phase-shift analysis procedure of Allen and co-workers,[51,52] but even here caution must still be exercised. In any event, the overall comparison between theory and experiment for energies in the 10–100 eV range and between the theoretical results themselves, on the elastic ICS, is largely favourable, making the derivation of an accurate recommended ICS for elastic scattering (see Sec. 4) highly feasible here.

The first thing we notice about the summed electronic-state ICS (see Fig. 2) is that our OP result underestimates its magnitude, compared to the measured data,[1,8–11] our ROP results, the BSR results,[19] and the CCC results,[19] at all energies ≤100 eV. We believe that this observation reflects, at least in part, its semi-phenomenological approach in separating the summed discrete electronic-state cross sections from the total absorption (discrete + continuum processes) cross section actually calculated. As a consequence, we do not discuss it further here, and nor does it figure in constructing our recommended data for this process in Sec. 4. It is also apparent in Fig. 2 that for energies less than about 7 eV, our ROP calculation underestimates the magnitude of the near-threshold electronic-state cross sections. This is reminiscent of what we found in our recent investigation in beryllium,[53] and we believe it is due to a similar reason. Namely, there are some strong near-threshold resonance states, found in both the BSR and CCC computations,[19] which greatly enhance the magnitude of the 3^3P excitation cross section. As the present ROP calculation includes only a relatively small number of excited states and does not include closed excitation channels, hence it cannot replicate this type of resonance. Therefore, in constructing our recommended dataset for the summed electronic-state ICSs, see Sec. 4, we prefer the BSR and CCC results for energies below 7 eV. For energies above 7 eV, however, at least up to 60 eV, all the available data[1,8–11] support the present ROP result over the BSR and CCC results. Nonetheless, the same caveat we mentioned above in our discussion of deriving experimental ICS from DCS measured over a finite angular range also applies here. While the effect is not as drastic here, as the ICSs can be measured to scattering angles close to 0°, it must still be borne in mind when we come to form our recommended dataset. For energies between 60 and 100 eV, however, all the theoretical and available measured data are in good accord here (see Fig. 2) so that we can again approach forming a recommended ICS set for the summed electronic-states with some confidence (see Sec. 4).

Finally, in Fig. 3, let us consider the total ionisation cross section for electron–magnesium scattering. In this case, we

TABLE 2. A selection of the present ROP results ($\times 10^{-16}$ cm^2) for electron scattering from Mg

Energy (eV)	Elastic ($\times 10^{-16}$ cm^2)	Inelastic ($\times 10^{-16}$ cm^2)	TICS ($\times 10^{-16}$ cm^2)	MTCS ($\times 10^{-16}$ cm^2)
0.02	341.317	0	0	451.818
0.03	379.338	0	0	528.577
0.05	504.377	0	0	692.608
0.07	683.012	0	0	837.708
0.09	855.488	0	0	909.687
0.11	959.742	0	0	892.250
0.13	985.187	0	0	818.055
0.19	847.946	0	0	567.267
0.22	762.557	0	0	480.612
0.26	665.120	0	0	398.594
0.34	523.367	0	0	299.355
0.42	428.163	0	0	241.300
0.50	360.045	0	0	202.107
0.60	297.890	0	0	166.980
0.80	216.677	0	0	120.644
1.00	167.040	0	0	91.881
1.20	135.477	0	0	74.297
1.50	109.607	0	0	63.553
1.70	102.438	0	0	59.558
2.70	91.675	0	0	41.497
2.80	89.457 726	0.025 502	0	42.537 353
2.90	88.088 309	0.041 407	0	40.390 832
3.20	84.240 645	0.079 891	0	34.805 106
3.40	81.841 903	0.099 886	0	31.674 948
3.80	77.344 775	0.131 776	0	26.530 485
4.20	73.170 002	0.153 921	0	22.544 311
4.40	70.807 325	0.431 383	0	20.735 437
4.60	67.782 902	1.554 829	0	18.713 487
5.20	59.588 585	5.472 386	0	13.908 489
6.00	51.438 904	9.670 431	0	10.061 396
7.00	43.863 656	13.661 446	0	7.286 416
7.80	39.413 397	16.068 932	0.023 631	5.926 219
8.00	38.439 476	16.584 174	0.082 985	5.652 987
8.20	37.512 083	17.052 273	0.163 472	5.402 357
8.60	35.795 422	17.826 660	0.369 543	4.960 303
9.00	34.256 010	18.388 216	0.615 701	4.589 758
10.00	31.049 895	19.201 214	1.305 798	3.887 527
12.00	26.422 927	20.107 225	2.620 630	3.020 960
14.00	23.168 722	20.588 336	3.621 835	2.522 850
16.00	20.749 735	20.481 877	4.317 276	2.224 313
18.00	18.899 403	20.069 614	4.780 953	2.039 118
22.00	16.268 726	19.242 602	5.261 882	1.837 048
30.00	13.141 434	18.028 330	5.386 281	1.694 724
40.00	11.049 856	16.295 613	5.040 673	1.638 890
50.00	9.604 558	14.540 219	4.607 341	1.611 585
70.00	7.873 279	11.923 636	3.863 964	1.515 950
100.00	6.384 028	9.458 905	3.141 428	1.269 803
150.00	4.958 657	7.301 478	2.434 628	0.915 652
200.00	4.097 104	5.801 537	2.003 906	0.688 539
250.00	3.513 484	4.838 353	1.715 277	0.540 708
300.00	3.090 268	4.052 504	1.503 220	0.439 272
400.00	2.514 612	2.985 749	1.209 158	0.311 613
500.00	2.138 188	2.314 992	1.010 307	0.235 871
650.00	1.763 410	1.746 789	0.824 297	0.167 599
750.00	1.585 948	1.464 862	0.727 290	0.138 305
850.00	1.444 475	1.252 365	0.649 003	0.116 490
1000.00	1.278 008	1.018 388	0.556 102	0.092 738
1500.00	0.934 904	0.612 186	0.383 504	0.051 180
2000.00	0.742 996	0.417 093	0.282 650	0.032 946
2500.00	0.618 657	0.307 856	0.219 319	0.023 115
3000.00	0.530 613	0.239 202	0.176 172	0.017 150
3500.00	0.465 238	0.192 582	0.145 215	0.013 338
4000.00	0.414 534	0.159 159	0.122 203	0.010 699
4500.00	0.374 012	0.134 186	0.104 604	0.008 791
5000.00	0.340 860	0.114 932	0.090 826	0.007 364

TABLE 3. Our recommended elastic ICSs, summed electronic-state excitation ICSs, and the TICS for electron–Mg scattering (all in units of 10^{-16} cm^2) on a fine energy grid. The uncertainty on the elastic data is ±15%, the uncertainty on the summed electronic-state data is ±25%, and the uncertainty on the TICS is ±15%

Energy (eV)	Elastic ($\times 10^{-16}$ cm^2)	Inelastic ($\times 10^{-16}$ cm^2)	TICS ($\times 10^{-16}$ cm^2)
$2.000\,000 \times 10^{-2}$	21.1229		
$2.110\,000 \times 10^{-2}$	24.0914		
$2.220\,000 \times 10^{-2}$	27.0600		
$2.340\,000 \times 10^{-2}$	30.2984		
$2.470\,000 \times 10^{-2}$	33.8066		
$2.600\,000 \times 10^{-2}$	37.3149		
$2.740\,000 \times 10^{-2}$	41.0930		
$2.890\,000 \times 10^{-2}$	45.1410		
$3.050\,000 \times 10^{-2}$	49.4589		
$3.210\,000 \times 10^{-2}$	53.7767		
$3.380\,000 \times 10^{-2}$	58.3645		
$3.570\,000 \times 10^{-2}$	66.1743		
$3.760\,000 \times 10^{-2}$	74.4246		
$3.960\,000 \times 10^{-2}$	83.1813		
$4.180\,000 \times 10^{-2}$	94.3821		
$4.400\,000 \times 10^{-2}$	105.583		
$4.640\,000 \times 10^{-2}$	117.802		
$4.890\,000 \times 10^{-2}$	134.393		
$5.150\,000 \times 10^{-2}$	152.839		
$5.430\,000 \times 10^{-2}$	173.161		
$5.720\,000 \times 10^{-2}$	194.812		
$6.030\,000 \times 10^{-2}$	224.496		
$6.360\,000 \times 10^{-2}$	257.798		
$6.699\,999 \times 10^{-2}$	293.545		
$7.060\,000 \times 10^{-2}$	333.947		
$7.450\,000 \times 10^{-2}$	382.067		
$7.850\,000 \times 10^{-2}$	438.059		
$8.270\,000 \times 10^{-2}$	500.513		
$8.719\,999 \times 10^{-2}$	572.477		
$9.190\,001 \times 10^{-2}$	643.987		
$9.680\,001 \times 10^{-2}$	723.335		
0.102 000	799.637		
0.108 000	869.621		
0.113 000	921.324		
0.120 000	982.326		
0.126 000	998.228		
0.133 000	1007.32		
0.140 000	997.505		
0.147 000	970.676		
0.155 000	931.311		
0.164 000	879.077		
0.173 000	826.232		
0.182 000	774.835		
0.192 000	723.164		
0.202 000	674.815		
0.213 000	625.694		
0.225 000	581.788		
0.237 000	541.511		
0.250 000	504.605		
0.263 000	473.795		
0.277 000	444.800		
0.292 000	419.713		
0.308 000	392.956		
0.325 000	370.611		
0.342 000	350.207		
0.361 000	330.001		
0.380 000	312.814		
0.400 000	297.712		
0.422 000	283.871		
0.445 000	270.223		
0.469 000	260.873		
0.494 000	252.143		
0.521 000	243.061		
0.549 000	233.937		

TABLE 3. Our recommended elastic ICSs, summed electronic-state excitation ICSs, and the TICS for electron–Mg scattering (all in units of 10^{-16} cm^2) on a fine energy grid. The uncertainty on the elastic data is ±15%, the uncertainty on the summed electronic-state data is ±25%, and the uncertainty on the TICS is ±15%—Continued

Energy (eV)	Elastic ($\times 10^{-16}$ cm^2)	Inelastic ($\times 10^{-16}$ cm^2)	TICS ($\times 10^{-16}$ cm^2)
0.579 000	224.621		
0.610 000	215.791		
0.643 000	208.538		
0.678 000	200.708		
0.714 000	194.227		
0.753 000	187.510		
0.793 000	181.555		
0.836 000	176.727		
0.881 000	170.597		
0.929 000	166.352		
0.979 000	160.991		
1.030 00	157.816		
1.090 00	153.746		
1.150 00	149.134		
1.210 00	144.685		
1.270 00	140.607		
1.340 00	136.102		
1.410 00	131.840		
1.490 00	127.344		
1.570 00	123.702		
1.660 00	119.992		
1.750 00	116.589		
1.840 00	113.348		
1.940 00	109.770		
2.040 00	106.741		
2.150 00	104.308		
2.270 00	101.662		
2.390 00	99.021 4		
2.520 00	96.165 8		
2.660 00	93.094 7		
2.714 00		0.000 000	
2.720 00		1.685 10	
2.800 00	89.719 7	16.894 0	
2.950 00	78.629 2	23.821 3	
3.110 00	74.119 9	21.095 8	
3.280 00	71.465 9	18.871 7	
3.460 00	69.130 0	17.151 5	
3.640 00	66.954 6	15.792 9	
3.840 00	64.263 3	14.546 9	
4.050 00	62.712 7	13.464 9	
4.270 00	60.252 8	12.835 1	
4.500 00	58.323 3	12.234 0	
4.740 00	56.491 4	12.303 8	
5.000 00	53.980 6	13.099 4	
5.270 00	51.472 0	13.200 1	
5.550 00	49.641 8	13.218 4	
5.850 00	47.284 4	13.950 3	
6.170 00	45.467 1	13.294 2	
6.500 00	43.360 3	13.680 1	
6.850 00	41.560 8	13.723 6	
7.220 00	39.813 5	14.152 5	
7.610 00	37.981 2	14.937 2	
7.653 26			0.000 000
7.700 00			$7.200\,000 \times 10^{-2}$
8.020 00	36.117 3	15.639 2	
8.100 00			0.421 000
8.400 00			0.800 000
8.450 00	34.263 8	16.198 4	
8.910 00	32.360 4	16.414 8	
9.200 00			1.660 00
9.390 00	30.518 1	16.330 0	
9.700 00			2.210 00
9.900 00	28.678 2	15.977 6	2.320 00
10.400 0	27.401 5	15.898 2	

TABLE 3. Our recommended elastic ICSs, summed electronic-state excitation ICSs, and the TICS for electron–Mg scattering (all in units of 10^{-16} cm^2) on a fine energy grid. The uncertainty on the elastic data is ±15%, the uncertainty on the summed electronic-state data is ±25%, and the uncertainty on the TICS is ±15%—Continued

Energy (eV)	Elastic ($\times10^{-16}$ cm^2)	Inelastic ($\times10^{-16}$ cm^2)	TICS ($\times10^{-16}$ cm^2)
11.000 0	26.029 1	16.190 9	3.068 60
11.600 0	24.872 9	16.298 8	3.542 56
12.200 0	23.637 1	16.428 0	3.914 02
12.900 0	22.409 4	16.465 8	4.265 14
13.600 0	21.284 3	16.563 2	4.563 76
14.300 0	20.212 9	16.648 5	4.770 38
15.100 0	19.097 7	16.657 8	4.926 54
15.900 0	18.276 8	16.608 7	5.001 26
16.700 0	17.493 5	16.586 5	5.075 98
17.600 0	16.699 5	16.469 5	5.144 04
18.600 0	15.890 6	16.364 4	5.157 44
19.600 0	15.137 6	16.325 7	5.170 84
20.700 0	14.460 6	16.276 8	5.150 36
21.800 0	13.890 6	16.195 5	5.107 56
23.000 0	13.339 1	16.083 3	5.056 19
24.200 0	12.858 1	15.979 5	5.000 14
25.500 0	12.287 2	15.867 0	4.944 89
26.900 0	11.761 7	15.719 5	4.891 37
28.300 0	11.290 4	15.576 8	4.841 80
29.900 0	10.795 0	15.410 2	4.787 67
31.500 0	10.460 6	15.228 7	4.721 70
33.200 0	10.121 4	15.034 2	4.654 52
35.000 0	9.779 82	14.832 0	4.588 04
36.800 0	9.456 06	14.622 7	4.527 96
38.800 0	9.112 99	14.389 2	4.418 53
40.900 0	8.802 76	14.143 4	4.287 06
43.100 0	8.531 21	13.884 2	4.170 48
45.500 0	8.241 80	13.603 4	4.038 35
47.900 0	7.978 35	13.329 9	3.803 40
50.500 0	7.707 34	13.039 0	3.699 56
53.200 0	7.488 66	12.760 5	3.574 31
56.100 0	7.258 22	12.467 4	3.460 91
59.100 0	7.027 34	12.174 7	3.375 17
62.300 0	6.811 60	11.882 9	3.222 90
65.700 0	6.596 75	11.584 2	3.054 99
69.200 0	6.382 20	11.288 1	3.008 13
73.000 0	6.189 05	10.983 1	2.902 37
76.900 0	6.012 76	10.689 0	2.796 17
81.100 0	5.839 00	10.394 0	2.707 38
85.500 0	5.667 94	10.101 5	2.594 65
90.100 0	5.493 62	9.804 62	2.486 94
94.900 0	5.320 08	9.512 10	2.436 49
100.000		9.210 01	2.293 30
105.000			2.235 35
110.000		8.798 20	
111.000			2.090 45
117.000			2.064 52
120.000		8.310 80	
123.000			2.022 59
130.000		7.872 66	1.988 13
137.000			1.904 18
140.000		7.474 41	
145.000			1.838 14
150.000	4.017 31	7.109 35	
152.000			1.795 84
160.000		6.772 70	
161.000			1.738 36
169.000			1.670 07
170.000		6.460 89	
178.000			1.587 81
180.000		6.171 07	
188.000			1.537 79
190.000		5.901 07	
198.000			1.492 77

TABLE 3. Our recommended elastic ICSs, summed electronic-state excitation ICSs, and the TICS for electron–Mg scattering (all in units of 10^{-16} cm^2) on a fine energy grid. The uncertainty on the elastic data is ±15%, the uncertainty on the summed electronic-state data is ±25%, and the uncertainty on the TICS is ±15%—Continued

Energy (eV)	Elastic ($\times10^{-16}$ cm^2)	Inelastic ($\times10^{-16}$ cm^2)	TICS ($\times10^{-16}$ cm^2)
200.000	3.348 24	5.648 88	
209.000			1.426 97
220.000			1.361 52
225.000		5.185 18	
232.000			1.336 26
245.000			1.309 74
250.000		4.711 04	
258.000			1.265 07
272.000			1.204 75
275.000		4.301 64	
286.000			1.157 08
300.000	2.558 58	3.945 87	
302.000			1.120 58
318.000			1.086 62
325.000		3.635 06	
335.000			1.049 57
350.000		3.362 10	
353.000			1.012 27
372.000			0.976 589
375.000		3.121 07	
393.000			0.940 124
400.000	2.101 62	2.907 19	
414.000			0.906 552
425.000		2.716 52	
436.000			0.877 386
450.000		2.545 85	
460.000			0.857 267
475.000		2.392 46	
484.000			0.837 561
500.000	1.799 86	2.254 08	
511.000			0.815 234
538.000			0.792 355
550.000		2.078 28	
567.000			0.765 213
598.000			0.730 004
600.000		1.873 65	
630.000			0.695 072
650.000		1.700 83	
664.000			0.668 806
700.000	1.419 28	1.553 34	
750.000		1.426 32	0.575 150
800.000		1.317 27	
850.000		1.219 41	
870.000			0.503 220
900.000		1.134 31	
950.000		1.058 86	
1000.00	1.097 05	0.991 591	0.501 100
1150.00			0.443 020
1320.00			0.371 800
1500.00		0.596 078	
1520.00			0.335 330
1750.00			0.290 450
2000.00	0.651 880	0.406 118	
2010.00			0.250 710
2300.00			0.237 520
2500.00		0.299 755	
2650.00			0.211 220
3000.00	0.474 428	0.232 908	0.186 650
3500.00		0.187 515	0.156 250
4000.00		0.154 971	0.149 050
4500.00		0.130 655	
4600.00			0.130 600
5000.00	0.313 047	0.111 908	

have three independent sets of measured data,[14–16] all of which largely agree with one another to within their stated errors and over their common energy range, as well as the OP, ROP, CCC,[19] and BSR[19] theoretical results. It is clear from Fig. 3 that none of the existing theories are able to reproduce the measured data over the relevant energy ranges available for comparison. Best agreement, to within the experimental uncertainties, from threshold to about 60 eV is provided by the BSR(712) computation, although even this somewhat systematically underestimates the magnitude of the TICS in that energy regime. At higher energies, $E_0 \gtrsim 500$ eV, it is the present ROP result which best reproduces the measured TICS. However, for energies between ~50 and 500 eV, none of the theories are able to reproduce the measured TICS which suggests that further computational work is required here before a quantitative theoretical description is achieved for ionisation. As the JPL[14] and Belfast[16] groups have very good reputations for making absolute TICS measurements, our recommended data are formed from an average of their results (see Sec. 4).

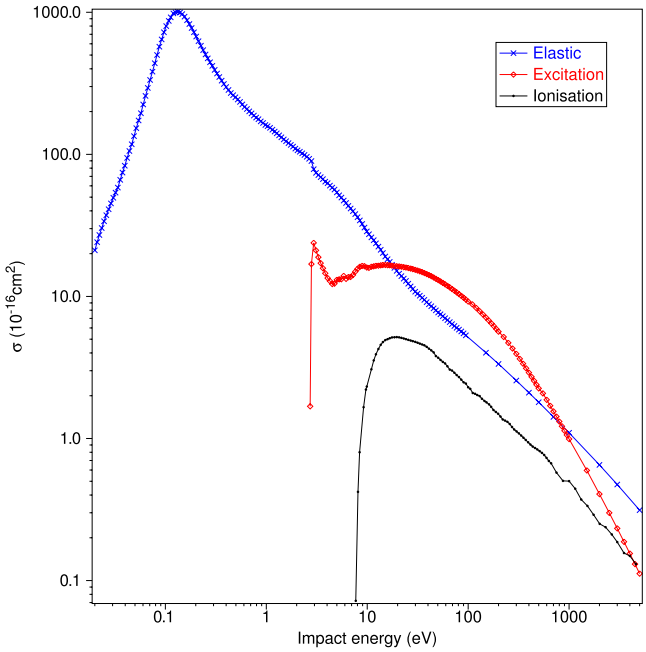

FIG. 4. Summary plot of our recommended cross section data ($\times 10^{-16}$ cm^2) for e^-–Mg scattering. See also the legend for further details.

4. Recommended Data

The recommended integral elastic cross section has been formed in the following manner. From 0.02 eV to 1.065 eV, this latter energy being where the ROP, OP, CCC(186) and BSR(48) all agree in cross section magnitude, we have employed the CCC(186) result. This is because we believe that at these lower energies, the close coupling calculations will be more accurate than those from the OP methods. In addition, as the CCC incorporates more basis sets (186 versus 48 for the BSR) than the BSR result, we expect it will be the more accurate of the two. From 1.065 eV to 100 eV, there is less to differentiate between all theoretical results so that we have taken an average of the OP, ROP, CCC, and BSR cross section values in order to determine the recommended data. Finally, for energies between 100 and 5000 eV, we have employed our OP data, scaled by a factor of 0.999933 to ensure continuity at 100 eV, to set the cross section values at those higher energies. A summary of our recommended elastic ICSs is given in Table 3, while a plot of it is incorporated into Fig. 4. Consistent with the philosophy outlined in Ref. 54, we assign an error, as we are dealing with a target which is not gaseous at room temperature, of ±15% on our recommended elastic ICS.

In the case of the summed electronic-state excitation cross sections, the BSR(712) are preferred (see the above discussion) for energies from threshold to 7.07 eV. Thereafter, between 7.07 and 100 eV, an average of the CCC(259), BSR (712), and our ROP cross sectionl results was used to generate the recommended data. Finally, for energies above 100 eV, the ROP ICS, suitably scaled by a factor of 0.973687 to ensure continuity at 100 eV, are employed to constitute our higher energy results. The excellent agreement between our ROP ICS and the BSR(712) ICS for energies between 80 and 200 eV (see Fig. 2) suggests that an appropriately scaled form of our ROP ICS can also be applied to extend all the individual discrete excitation process (e.g., $3^1S \rightarrow 3^1P$, $3^1S \rightarrow 3^3P$, and so on) cross sections in Ref. 19 to 5000 eV. This would provide an extra degree of precision for the modeling community over that afforded by the summed ICS data. Our recommended discrete electronic-state excitation ICSs are listed in Table 3 and plotted in Fig. 4. Following Buckman *et al.*[54] again, we ascribe uncertainties on our recommended ICS here to be ±25%.

As discussed above in Sec. 3, none of the available theories provide an adequate description of the TICS from threshold to 5000 eV. On the other hand, there are well-regarded measurements from Refs. 16 and 14 that, over their common energy range and to within their stated uncertainties, are in very good agreement with one another. As a consequence, we have formed our recommended TICS from threshold to about 10 eV using Ref. 16, an average of the cross sections from Refs. 14 and 16 from ~10 eV to 700 eV, and finally the TICS from Ref. 16 above 700 eV. These data are also listed in Table 3 and plotted in Fig. 4. Consistent with the uncertainties on the available Mg TICS[14–16] and recent measurements of the TICS for species that are not gaseous at room temperatures,[55–57] we estimate the uncertainties on the present TICS to be ±15%.

In Fig. 5, we present the results for the drift velocity, W, characteristic energy, D_T/μ (where D_T is the transverse diffusion coefficients and μ is the mobility), and the reduced ionisation rate, k, for an electron swarm in Mg vapour over the range of reduced fields, E/n_0, from 0.1 to 1000 Td, where n_0 is the neutral density. The results in Fig. 5 compare the transport coefficients calculated using both the ROP and the recommended cross section sets. In all calculations for both sets, we have assumed isotropic scattering in the inelastic and ionisation channels utilising the relevant integral cross sections for these processes. We have considered the anisotropic

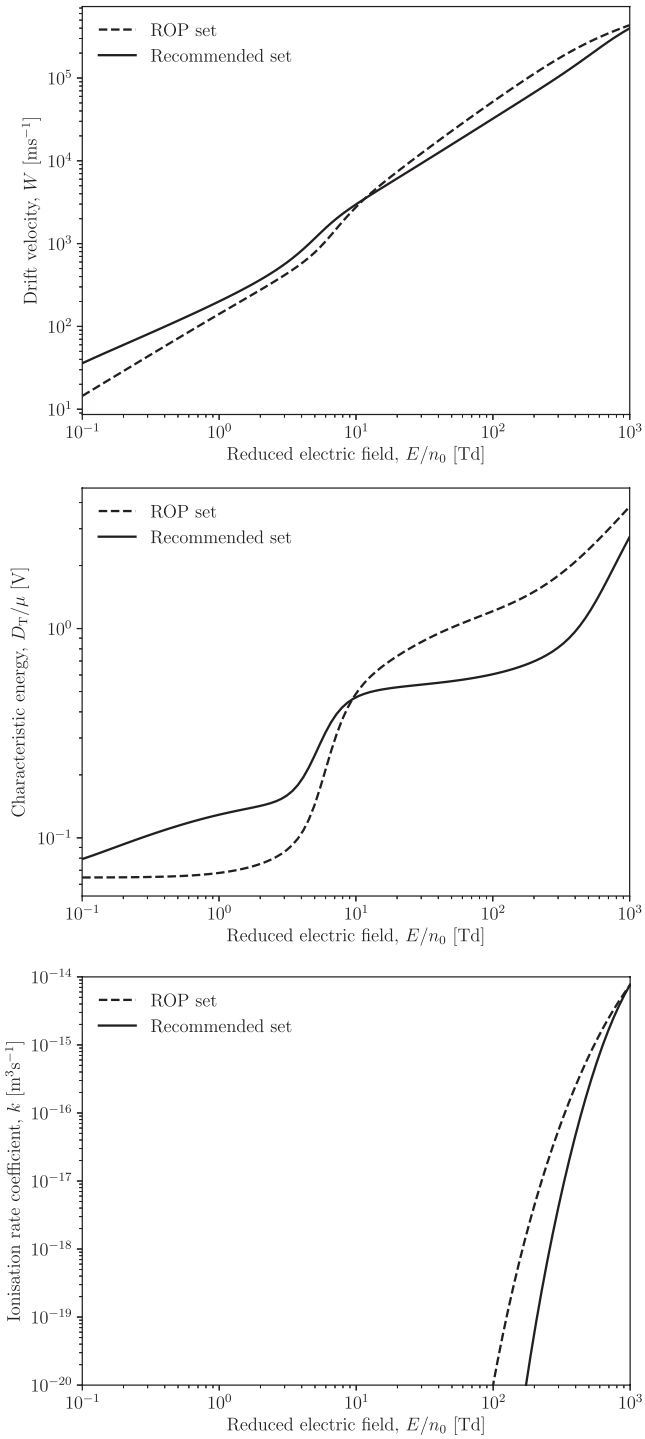

FIG. 5. Comparison of the calculated flux drift velocities (top), characteristic energies D_T/μ (middle), and ionisation rate coefficients (bottom), for electrons in Mg gas at 750 K over a range of reduced electric fields using the ROP and recommended cross section sets. See also the legend for further details.

nature of elastic scattering at the level of the MTCS in both cases. The elastic MTCS for the ROP is implemented directly as per Table 2, while for the recommended set, we have assumed the form of differential cross section for the ROP method to scale the recommended integrated elastic cross section to obtain the recommended elastic MTCS. The gas temperature is fixed at 750 K, which aligns with the gas temperatures used in the gas phase measurements.[14–16] Transport coefficients are calculated using a well benchmarked multi-term solution of Boltzmann's equation.[27] In these calculations for electrons in gaseous Mg, we have found that the two-term approximation[58,59] can be in error by as much as 30% (in the diffusion coefficient) at the higher E/n_0 region considered.

For reduced fields up to 1-2 Td, electrons are essentially in thermal equilibrium with the Mg gas, and in this regime, the electron transport is essentially governed by elastic scattering processes. The reduced drift velocity of the ROP set compared to the recommended set in this region is a reflection of the enhanced elastic cross section in the low energy region as shown in Fig. 1. Furthermore, we observe that the characteristic energy for the recommended set rises much slower with increasing field in the intermediate field region due to the enhanced inelastic cross section near threshold of the recommended summed inelastic channels. These enhanced inelastic scattering processes in the recommended set consequently enhance the field required for the onset of ionisation as compared with the ROP set. For fields higher than 1000 Td, there is a general convergence in the transport coefficients calculated for the two different cross section sets. Please note that a definitive swarm analysis would require us to include all the individual excited-state electronic channels. The aim of this swarm study, however, was to highlight the sensitivity of the transport data to the input cross sections (see Fig. 5). For this, the inclusion of the summed ICSs, both from our calculations and from our recommended data, was sufficient. If experimental swarm data for Mg were to become available in the future, we note that all individual electronic excitation channels would need to be considered.

5. Conclusions

We have reported new OP and ROP theoretical results for the electron–magnesium scattering system. Specifically, integral elastic cross sections, integral cross sections for the summed electronic-state excitations and the total ionisation cross sections were computed over a wide energy range and compared against the corresponding previous measurements and other calculations. As a result of these comparisons, a set of recommended cross section data, with uncertainty estimates, has been compiled for each of these same processes, with those data being very useful for modellers seeking to simulate systems in which magnesium is a constituent and electron scattering relevant. We consequently presented a brief study of the electron transport in Mg gas at 750 K and showed that the transport coefficients are quite sensitive to the cross section set. This will hopefully motivate future swarm experiments for this system.

Acknowledgments

This work was financially supported, in part, by the Spanish Ministerio de Ciencia, Innovacion y Universidades (Project No. FIS2016-80440) and the Australian Research Council (Project Nos. DP160102787 and DP180101655). We thank

Dr. L. Campbell for his help with some aspects of this study, while one of us (M.J.B.) thanks CSIC for its hospitality during a recent visit. We also acknowledge helpful conversations with Professor K. Bartschat. Finally, we also thank Dr. O. Zatsarinny and Professor K. Bartschat for providing us tables of their BSR data and Professor I. Bray for the CCC data.

6. References

[1]W. Williams and S. Trajmar, J. Phys. B: At. Mol. Phys. **11**, 2021 (1978).
[2]M. J. Brunger, R. K. Houghton, and P. J. O. Teubner, Aust. J. Phys. **48**, 71 (1995).
[3]M. J. Brunger, J. L. Riley, R. E. Scholton, and P. J. O. Teubner, J. Phys. B: At., Mol. Opt. Phys. **21**, 1639 (1988).
[4]R. K. Houghton, M. J. Brunger, G. Shen, and P. J. O. Teubner, J. Phys. B: At., Mol. Opt. Phys. **27**, 3573 (1994).
[5]D. O. Brown, D. Cvejanovic, and A. Crowe, J. Phys. B: At., Mol. Opt. Phys. **36**, 3411 (2003).
[6]D. O. Brown, A. Crowe, D. V. Fursa, I. Bray, and K. Bartschat, J. Phys. B: At., Mol. Opt. Phys. **38**, 4123 (2005).
[7]B. Predojević, V. Pejčev, D. M. Filipović, D. Sević, and B. P. Marinković, J. Phys. B: At., Mol. Opt. Phys. **40**, 1853 (2007).
[8]D. M. Filipović, B. Predojević, D. Sević, V. Pejčev, B. P. Marinković, R. Srivastava, and A. D. Stauffer, Int. J. Mass Spectrom. **251**, 66 (2006).
[9]D. M. Filipović, B. Predojević, V. Pejčev, D. Sević, B. P. Marinković, R. Srivastava, and A. D. Stauffer, J. Phys. B: At., Mol. Opt. Phys. **39**, 2583 (2006).
[10]B. Predojević, V. Pejčev, D. M. Filipović, D. Sević, B. Tomčik, and B. P. Marinković, J. Phys. B: At., Mol. Opt. Phys. **44**, 055208 (2011).
[11]B. Predojević, V. Pejčev, D. M. Filipović, D. Sević, and B. P. Marinković, J. Phys. B: At., Mol. Opt. Phys. **41**, 015202 (2008).
[12]M. J. Brunger, J. L. Riley, R. E. Scholten, and P. J. O. Teubner, J. Phys. B: At., Mol. Opt. Phys. **22**, 1431 (1989).
[13]J. Pursehouse, C. Bostock, K. Nixon, M. Harvey, D. V. Fursa, I. Bray, and A. J. Murray, Phys. Rev. A **98**, 022702 (2018).
[14]R. F. Boivin and S. K. Srivastava, J. Phys. B: At., Mol. Opt. Phys. **31**, 2381 (1998).
[15]R. S. Freund, R. C. Wetzel, R. J. Shul, and T. R. Hayes, Phys. Rev. A **41**, 3575 (1990).
[16]P. McCallion, M. B. Shah, and H. B. Gilbody, J. Phys. B: At., Mol. Opt. Phys. **25**, 1051 (1992).
[17]O. Zatsarinny and K. Bartschat, Phys. Rev. A **79**, 052709 (2009).
[18]K. Bartschat, O. Zatsarinny, I. Bray, D. V. Fursa, and A. T. Stelbovics, J. Phys. B: At., Mol. Opt. Phys. **37**, 2617 (2004).
[19]P. S. Barklem, Y. Osorio, D. V. Fursa, I. Bray, O. Zatsarinny, K. Bartschat, and A. J. Jerkstrand, Astron. Astrophys. **606**, A11 (2017).
[20]I. Bray, K. McNamara, and D. V. Fursa, Phys. Rev. A **92**, 022705 (2015).
[21]M. Ismail Hossain, A. K. F. Haque, M. Atiqur, R. Patoary, M. A. Uddin, and A. K. Basak, Eur. Phys. J. D **70**, 41 (2016).
[22]Y. Osorio and P. S. Barklem, Astron. Astrophys. **586**, A120 (2016).
[23]Ø. Langangen and M. Carlsson, Astrophys. J. **696**, 1892 (2009).
[24]M. Vieytes, P. Mauas, C. Cacciari, L. Origlia, and E. Pancino, Astron. Astrophys. **526**, A4 (2011).
[25]A. Jerkstrand, M. Ergon, S. J. Smartt, C. Fransson, J. Sollerman, S. Taubenberger, M. Bersten, and J. Spyromilio, Astron. Astrophys. **573**, A12 (2015).
[26]H. Tanaka, M. J. Brunger, L. Campbell, H. Kato, M. Hoshino, and A. R. P. Rau, Rev. Mod. Phys. **88**, 025004 (2016).
[27]R. D. White, D. Cocks, G. Boyle, M. Casey, N. Garland, D. Konovalov, B. Philippa, P. Stokes, J. de Urquijo, O. González-Magaña, R. P. McEachran, S. J. Buckman, M. J. Brunger, G. Garcia, S. Dujko, and Z. Lj. Petrovic, Plasma Sources Sci. Technol. **27**, 053001 (2018).
[28]M. J. E. Casey, J. de Urquijo, L. N. Serkovu Loli, D. G. Cocks, G. J. Boyle, D. B. Jones, M. J. Brunger, and R. D. White, J. Chem. Phys. **147**, 195103 (2017).
[29]G. J. Boyle, R. P. McEachran, D. G. Cocks, M. J. Brunger, S. J. Buckman, S. Dujko, and R. D. White, J. Phys. D: Appl. Phys. **49**, 355201 (2016).
[30]M. J. Brunger, Int. Rev. Phys. Chem. **36**, 333 (2017).
[31]M. C. Fuss, L. Ellis-Gibbings, D. B. Jones, M. J. Brunger, F. Blanco, A. Muñoz, P. Limão-Vieira, and G. García, J. Appl. Phys. **117**, 214701 (2015).
[32]M. J. Brunger, K. Ratnavelu, S. J. Buckman, D. B. Jones, A. Muñoz, F. Blanco, and G. García, Eur. Phys. J. D **70**, 46 (2017).
[33]L. Campbell and M. J. Brunger, Int. Rev. Phys. Chem. **35**, 297 (2016).
[34]L. Campbell and M. J. Brunger, Plasma Sources Sci. Technol. **22**, 013002 (2013).
[35]F. Blanco and G. García, Phys. Lett. A **255**, 147 (1999).
[36]F. Blanco and G. García, Phys. Lett. A **295**, 178 (2002).
[37]F. Blanco and G. García, Phys. Rev. A **67**, 022701 (2003).
[38]F. Blanco, F. Ferreira da Silva, P. Limão-Vieira, and G. García, Plasma Sources Sci. Technol. **26**, 085004 (2017).
[39]G. Staszewska, D. W. Schwenke, D. Thirumalai, and D. G. Truhlar, Phys. Rev. A **28**, 2740 (1983); J. Phys. B: At. Mol. Phys. **16**, L281 (1983).
[40]https://physics.nist.gov/PhysRefData/ASD/lines_form.html.
[41]S. Chen, R. P. McEachran, and A. D. Stauffer, J. Phys. B: At., Mol. Opt. Phys. **41**, 025201 (2008).
[42]K. Bartschat, R. P. McEachran, and A. D. Stauffer, J. Phys. B: At., Mol. Opt. Phys. **21**, 2789 (1988).
[43]K. Bartschat, R. P. McEachran, and A. D. Stauffer, J. Phys. B: At., Mol. Opt. Phys. **23**, 2349 (1990).
[44]R. P. McEachran, D. L. Morgan, A. G. Ryman, and A. D. Stauffer, J. Phys. B: At. Mol. Phys. **10**, 663 (1977).
[45]R. P. McEachran, D. L. Morgan, A. G. Ryman, and A. D. Stauffer, J. Phys. B: At. Mol. Phys. **11**, 951 (1978).
[46]R. P. McEachran and A. D. Stauffer, J. Phys. B: At., Mol. Opt. Phys. **23**, 4605 (1990).
[47]D. J. R. Mimnagh, R. P. McEachran, and A. D. Stauffer, J. Phys. B: At., Mol. Opt. Phys. **26**, 1727 (1993).
[48]S. Chattopadhyay, B. K. Mani, and D. Angom, Phys. Rev. A **89**, 022506 (2014).
[49]S. J. Buckman and C. W. Clark, Rev. Mod. Phys. **66**, 539 (1994).
[50]P. D. Burrow, J. A. Michejdo, and J. Lower, J. Phys. B: At. Mol. Phys. **9**, 3225 (1976).
[51]L. J. Allen, M. J. Brunger, I. E. McCarthy, and P. J. O. Teubner, J. Phys. B: At. Mol. Phys. **20**, 4861 (1987).
[52]M. J. Brunger, S. J. Buckman, L. J. Allen, I. E. McCarthy, and K. Ratnavelu, J. Phys. B: At., Mol. Opt. Phys. **25**, 1823 (1992).
[53]R. P. McEachran, F. Blanco, G. García, and M. J. Brunger, J. Phys. Chem. Ref. Data **47**, 033103 (2018).
[54]S. J. Buckman, M. J. Brunger, and K. Ratnavelu, Fusion Sci. Technol. **63**, 385 (2013).
[55]K. L. Nixon, W. A. D. Pires, R. F. C. Neves, H. V. Duque, D. B. Jones, M. J. Brunger, and M. C. A. Lopes, Int. J. Mass Spectrom. **404**, 48 (2016).
[56]W. A. D. Pires, K. L. Nixon, S. Ghosh, R. F. C. Neves, H. V. Duque, R. A. A. Amorim, D. B. Jones, F. Blanco, G. Garcia, M. J. Brunger, and M. C. A. Lopes, Int. J. Mass Spectrom. **422**, 32 (2017).
[57]S. Ghosh, K. L. Nixon, W. A. D. Pires, R. A. A. Amorim, R. F. C. Neves, H. V. Duque, D. G. M. da Silva, D. B. Jones, F. Blanco, G. Garcia, M. J. Brunger, and M. C. A. Lopes, Int. J. Mass Spectrom. **430**, 44 (2018).
[58]G. J. Boyle, W. J. Tattersall, D. G. Cocks, R. P. McEachran, and R. D. White, Plasma Sources Science and Technology **26**, 024007 (2017).
[59]R. D. White, R. E. Robson, B. Schmidt, and M. A. Morrison, J. Phys. D: Appl. Phys. **36**, 3125 (2003).